Asymmetry-enhanced phase sensing via asymmetric entangled coherent states

Xiao-Tong Chen,[1] Rui Zhang,[1] Wang-Jun Lu,[2,*] Yunlan Zuo,[1] Ya-Feng Jiao,[3,†] and Le-Man Kuang[1,3,‡]

[1]*Key Laboratory of Low-Dimensional Quantum Structures and Quantum Control of Ministry of Education, Synergetic Innovation Center for Quantum Effects and Applications, XJ-Laboratory and Department of Physics, Hunan Normal University, Changsha 410081, China*

[2]*Department of Maths and Physics, Hunan Institute of Engineering, Xiangtan 411104, China*

[3]*Academy for Quantum Science and Technology, Zhengzhou University of Light Industry, Zhengzhou 450002, China*

(Received 29 August 2023; revised 8 February 2024; accepted 19 March 2024; published 4 April 2024)

We study quantum phase sensing with asymmetric two-mode entangled coherent states (ECSs) in which the two local amplitudes take different values. We find the asymmetry-enhanced phase-sensing phenomenon in which the phase-sensing sensitivity is enhanced with increasing the asymmetry in the ECSs. We indicate that the phase-sensing sensitivity can attain and even surpass the Heisenberg limit in certain regimes of parameters. We further study the effect of decoherence induced by photon loss on the phase-sensing sensitivity. It is shown that the asymmetric ECSs have greater capability against decoherence compared with the symmetric ECSs. It is indicated that the asymmetric ECSs have significant advantages over the symmetric ECSs in quantum phase sensing. We also study the practical phase-sensing scheme with the intensity-difference measurement and show that the asymmetry in the asymmetric ECSs can enhance the phase sensitivity in the practical phase-measurement scheme. Our work reveals the asymmetry in the asymmetric ECSs is a resource for quantum-enhanced sensing and may be applied to ultrasensitive quantum phase sensing in the presence of photon loss.

DOI: 10.1103/PhysRevA.109.042609

I. INTRODUCTION

Entangled coherent states (ECSs) [1–5] as a kind of significant quantum resource of continuous variables have many potential applications in fundamental tests of quantum physics and quantum information processing such as Bell-inequality tests [6–8], tests for nonlocal realism [9,10], quantum teleportation [11–15], quantum computation [16–22], quantum key distribution [23], and quantum precision measurements [24–32]. An optical four-component ECS [33] was experimentally prepared by using of a very lossy quantum channel. A two-mode ECS was experimentally realized by using a Mach-Zehnder interferometer (MZI) equipped with a cross-Kerr element in each of two spatially separated modes [34]. A number of schemes for the implementation of ECSs in various quantum systems have been proposed [35–48].

Enhancing the precision of a measured parameter is always a basic topic in quantum metrology [49–55]. Quantum states of light can improve the sensitivity of phase measurements beyond the limits that apply to classical light sources. The phase sensitivity of classical light is limited by the shot noise of independent photon-detection events to the standard quantum limit (SQL) of $\delta\phi = 1/\sqrt{N}$, with N being the number of photons. Quantum mechanics imposes limits to the measurement precision. Conventional measurement techniques typically fail to reach these quantum limits. For instance, the SQL can be overcome by using the multiphoton coherences of nonclassical light. Conventional bounds to the precision of measurements such as the SQL are not as fundamental as the Heisenberg limit of $\delta\phi = 1/N$ from the Heisenberg uncertainty principle and can be beaten by using quantum strategies. Quantum-enhanced metrology studies how to exploit quantum resources, such as squeezing, entanglement, and quantum phase transition, to overcome the SQL and to exhibit quantum advantages [56–77].

Phase estimation is a ubiquitous measurement primitive, used for precision measurement of length, displacement, speed, optical properties, and so on. Precise phase estimation is of particular significance for various applications such as imaging, sensing, and information processing. Caves [78] proposed the first squeezing-enhanced interferometer scheme for phase sensing by taking a high-intensity coherent state and a low-intensity squeezed vacuum state as the input states of the interferometer, which showed that the precision of phase estimation can beat the SQL. This principle is widely used in gravitational-wave observatories to enhance precision beyond the limits of classical technology [79,80]. Since Caves's scheme of quantum phase sensing, many protocols have been proposed to improve the precision of phase estimation, such as NOON states [81–83], entangled coherent states [28], two-mode squeezed states [84], number squeezed states [85], and so on.

The NOON-type ECS $|\alpha\rangle|0\rangle + |0\rangle|\alpha\rangle$, which is a specific coherent superposition of the NOON states, was proposed as the input state of the MZI phase-measurement scheme to enhance the precision of phase sensing [28,30,31]. It was shown that the phase-sensing precision of the NOON-type ECS scheme can surpass that of the NOON state in both the absence and presence of photon loss. In general, a

*wjlu1227@zju.edu.cn
†yfjiao@hunnu.edu.cn
‡lmkuang@hunnu.edu.cn

two-mode ECS with components $|\alpha_1, \beta_1\rangle + |\alpha_2, \beta_2\rangle$ is called a symmetric ECS when it remains invariant after exchanging the state parameters of the two modes, i.e., $|\alpha_1, \beta_1\rangle + |\alpha_2, \beta_2\rangle = |\beta_1, \alpha_1\rangle + |\beta_2, \alpha_2\rangle$. Otherwise, it is an asymmetric ECS, i.e., $|\alpha_1, \beta_1\rangle + |\alpha_2, \beta_2\rangle \neq |\beta_1, \alpha_1\rangle + |\beta_2, \alpha_2\rangle$. The NOON-type ECS is just a specific example of the symmetric two-mode ECS $|\alpha\rangle|\beta\rangle + |\beta\rangle|\alpha\rangle$.

Recently, it was demonstrated that the symmetric ECS $|\alpha\rangle|\beta\rangle + |\beta\rangle|\alpha\rangle$ is the optimal ECS with respect to the separable coherent state $|\alpha\rangle|\beta\rangle$ for quantum phase estimation in lossy interferometry [32] under the constraint of the same input mean photon number. Entanglement in the symmetric ECS is the critical. reason to attribute to enhancing the phase sensitivity. On the other hand, it is noted that the ECS, $|\alpha, \beta\rangle + |-\alpha, -\beta\rangle$, is an asymmetric ECS when $\alpha \neq \beta$, which is not invariant under the exchange of the state parameters α and β. It becomes the symmetric ECS $|\alpha\rangle|\alpha\rangle + |-\alpha\rangle|-\alpha\rangle$ when $\alpha = \beta$. As is well known, quantum nonlocality is a powerful resource for quantum information processing. It was found that the asymmetric ECS has obvious advantages over the symmetric ECS in testing the Bell-Clauser-Horne-Shimony-Holt inequality and can significantly increase the violation of the inequality [8]. This implies that the asymmetric ECS has stronger quantum nonlocality than the symmetric ECS. Asymmetry-enhanced quantum nonlocality of the asymmetric ECS inspires an interesting question, whether the asymmetry of the asymmetric ECS can improve the sensitivity of quantum phase sensing.

In this paper, we study quantum phase sensing based on the asymmetric ECS $|\alpha, \beta\rangle + |-\alpha, -\beta\rangle$ and show how to effectively enhance the phase sensitivity by using the asymmetric ECS. We find that the asymmetry of the asymmetric ECS can significantly enhance the phase-sensing precision compared with the symmetric ECS under the constraint of the same input mean photon number. Furthermore, we show that the asymmetric ECSs have greater capability against decoherence induced by photon loss compared with the symmetric ECS. It is indicated that the asymmetric ECSs have obvious advantages over the symmetric ECSs in quantum phase sensing. We also study the practical phase-sensing scheme with the intensity-difference measurement and show that the asymmetry in the asymmetric ECS can enhance the phase sensitivity in the practical phase-measurement scheme.

This paper is structured as follows. In Sec. II, we study the quantum phase sensing with asymmetric ECSs via the MZI in the absence of photon loss. In Sec. III, we investigate the quantum phase sensing with asymmetric ECSs under the effect of decoherence induced by photon loss. In Sec. IV, we discuss the quantum phase sensing in an optical intensity-difference-measurement scheme with an asymmetric two-mode ECS. Finally, our conclusions are summarized in Sec. V.

II. ASYMMETRY-ENHANCED PHASE SENSING WITH ASYMMETRIC ECSs WITHOUT PHOTON LOSS

In this section, we study asymmetry-enhanced phase sensing with asymmetric ECSs in the absence of photon loss with the photon-loss rate $R = 0$. We will show that the performance

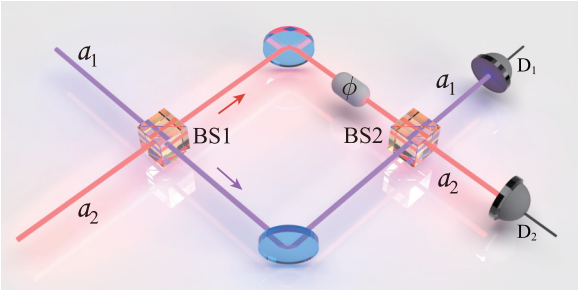

FIG. 1. Schematic of the quantum phase sensing with the Mach-Zehnder interferometer. BS, beam splitter.

of the asymmetric ECS can surpass that of the symmetric ECS in the quantum phase estimation.

The MZI is a well-known optical device in quantum metrology. We consider the MZI scheme of the quantum phases sensing [27] in which the MZI is constructed with two 50:50 beam splitters and one phase shift in one arm, as shown in Fig. 1. We study quantum phase sensing with the input sensor state after the first beam splitter being the following two-component ECS:

$$|\Psi\rangle = N(|\alpha\rangle_1|k\alpha\rangle_2 + |-\alpha\rangle_1|-k\alpha\rangle_2) \quad (k \neq 0), \tag{1}$$

where $|\pm\alpha\rangle_1$ and $|\pm k\alpha\rangle_2$ are coherent states with amplitudes $\pm\alpha$ and $\pm k\alpha$ for the first and second sensor modes, respectively. k is an arbitrary nonzero real number. The normalization constant is given by

$$N = \left[2 + 2e^{-2(1+k^2)|\alpha|^2}\right]^{-1/2}. \tag{2}$$

We can see that the ECS given by Eq. (1) is the symmetric ECS when $k = \pm 1$. However, the ECS given by Eq. (1) is the asymmetric ECS when $k \neq \pm 1$. In what follows we will show that the asymmetry of the asymmetric ECS would be a quantum resource to exhibit the quantum advantage of the quantum phase sensing.

In order to investigate achievable phase sensitivity with the asymmetric ECS, we directly evaluate the quantum Fisher information (QFI) of the output state of the MZI sensor after phase accumulation with the following expression:

$$\begin{aligned} |\Psi(\phi)\rangle &= e^{i\phi\hat{n}_2}|\Psi\rangle \\ &= N[|\alpha\rangle_1|e^{i\phi}k\alpha\rangle_2 + |-\alpha\rangle_1|-e^{i\phi}k\alpha\rangle_2], \end{aligned} \tag{3}$$

where $\hat{n}_2 = \hat{a}_2^\dagger\hat{a}_2$ is the photon number operator of the second sensor mode.

The QFI of the output state of the phase sensor $|\Psi(\phi)\rangle$ with respect to the phase parameter ϕ is given by

$$F_Q = 4[\langle\Psi'(\phi)|\Psi'(\phi)\rangle - |\langle\Psi'(\phi)|\Psi(\phi)\rangle|^2], \tag{4}$$

where the derivative is given by

$$|\Psi'(\phi)\rangle = \frac{\partial}{\partial\phi}|\Psi(\phi)\rangle = i\hat{n}_2|\Psi(\phi)\rangle. \tag{5}$$

Then we can obtain

$$F_Q = 4\left[\langle\hat{n}_2^2\rangle - (\langle\hat{n}_2\rangle)^2\right], \tag{6}$$

where the expectation values are taken with respect to the sensor input state $|\Psi\rangle$ given by Eq. (1).

We note that the phase sensitivity should be determined by the relation between the QFI and the total mean photon number in the input state of the two sensor modes $|\Psi\rangle$. The total photon number operator is $\hat{n} = \hat{n}_1 + \hat{n}_2$, with $\hat{n}_1 = \hat{a}_1^\dagger \hat{a}_1$ being the photon number operator of the first sensor mode. It is straightforward to obtain the following the expectation values of the photon number operators in the input state $|\Psi\rangle$ given by Eq. (1):

$$\langle \hat{n}_1 \rangle = |\alpha|^2 \frac{1 - e^{-2|\alpha|^2(1+k^2)}}{1 + e^{-2|\alpha|^2(1+k^2)}}, \tag{7}$$

$$\langle \hat{n}_2 \rangle = k^2|\alpha|^2 \frac{1 - e^{-2|\alpha|^2(1+k^2)}}{1 + e^{-2|\alpha|^2(1+k^2)}}, \tag{8}$$

$$\langle \hat{n} \rangle = (1 + k^2)|\alpha|^2 \frac{1 - e^{-2|\alpha|^2(1+k^2)}}{1 + e^{-2|\alpha|^2(1+k^2)}}. \tag{9}$$

Then we have

$$\langle \hat{n}_1 \rangle = \frac{1}{1+k^2}\langle \hat{n} \rangle, \quad \langle \hat{n}_2 \rangle = \frac{k^2}{1+k^2}\langle \hat{n} \rangle. \tag{10}$$

Similarly, we can get the following expectation values:

$$\langle \hat{n}_2^2 \rangle = \frac{k^2}{1+k^2}\langle \hat{n} \rangle + k^4|\alpha|^4, \tag{11}$$

$$\langle \hat{n}_1^2 \rangle = \frac{1}{1+k^2}\langle \hat{n} \rangle + |\alpha|^4, \tag{12}$$

$$\langle \hat{n}^2 \rangle = \langle \hat{n} \rangle + (1 + k^2)^2|\alpha|^4. \tag{13}$$

Substituting Eqs. (10)–(13) in Eq. (6), we can express the QFI of the output state of the MZI sensor $|\Psi(\phi)\rangle$ in terms of the total mean photon number and its covariance as

$$F_Q = \left(\frac{2k}{1+k^2}\right)^2 [\langle \hat{n} \rangle + k^2(\Delta \hat{n})^2], \tag{14}$$

where $\langle \hat{n} \rangle$ and $(\Delta \hat{n})^2$ are the expectation value and the covariance of the total photon number operator in the input state of the phase sensor $|\Psi\rangle$ given by Eq. (1).

It is interesting to note that a higher phase sensitivity can be attained in the larger asymmetric regime. Indeed, from Eq. (14) we obtain $F_Q \approx \frac{4}{k^2}[\langle \hat{n} \rangle + k^2(\Delta \hat{n})^2]$ in the large asymmetric regime of $k \gg 1$. The ultimate precision of the phase sensitivity is given by the quantum Cramér-Rao bound $\delta\phi_{\min} = 1\sqrt{F_Q}$, so we can find the ultimate precision with the following expression:

$$\delta\phi_{\min} \approx \frac{k}{2\sqrt{\langle \hat{n} \rangle + k^2(\Delta \hat{n})^2}}, \tag{15}$$

which indicates that the phase-sensitivity limit may surpass the SQL and reach the sub-Heisenberg or even Heisenberg limit.

In Fig. 2, we plot the QFI with respect to the mean photon number $\bar{n}$ for different values of the asymmetric parameter. The dotted, dash-dotted, and dashed lines correspond to $k = 1, 2$, and 10, respectively. The solid line denotes the QFI at the SQL ($F_Q = \bar{n}$). Note that the case with $k = 1$ corresponds to the symmetric ECS. From Fig. 2, we can observe that the QFI in the whole asymmetric-parameter regime of $k > 1$ is always larger than the QFI of the SQL. And the QFI of the asymmetric ECS ($k > 1$) is larger than that of the symmetric ECS ($k = 1$) under the constraint condition of the same input mean photon number $\bar{n}$. This implies that the phase-sensitivity limit $\delta\phi_{\min}$ of the asymmetric ECS is lower than that of the symmetric ECS. In particular, Fig. 2 indicates that in the small mean-photon-number regime of about $\bar{n} < 3$, we find $F_Q \sim \bar{n}^2$. So we have phase sensitivity $\delta\phi_{\min} \sim 1/\bar{n}$ because $\delta\phi_{\min} = 1/\sqrt{F_Q}$. This means that the Heisenberg limit of the phase sensitivity is attainable in the small mean-photon-number regime. Therefore, we can conclude that the asymmetry of the sensor input state can enhance the phase-sensitivity limit.

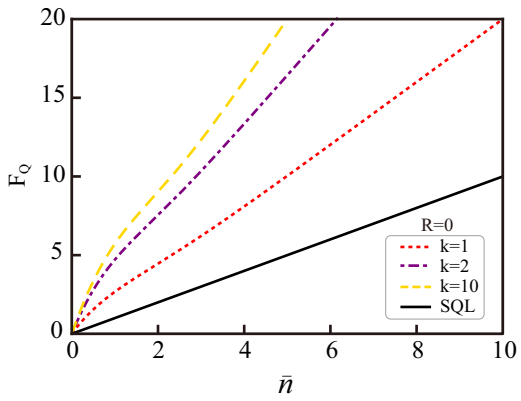

FIG. 2. The QFI with respect to the total mean photon number $\bar{n}$ in the absence of photon loss ($R = 0$). The dotted, dash-dotted, and dashed lines correspond to $k = 1, 2$, and 10, respectively. The solid line denotes the QFI at the SQL.

In order to further demonstrate the sensitivity limit of the asymmetric ECS in the phase estimation, in Table I we list some representative data for the QFI and the total mean photon number $\bar{n}$ and its square $\bar{n}^2$ when $k = 10$. From the data in Table I, we find $\delta\phi_{\min} < 1/\bar{n}$ when $1 < \bar{n} \leqslant 4$ because $F_Q > \bar{n}^2$. This implies that the phase-sensitivity limit of the asymmetric ECS can surpass the Heisenberg limit in the regime of the small photon number. In the regime of $\bar{n} > 4$, we find $\bar{n} < F_Q < \bar{n}^2$, which indicates that the phase-sensitivity limit of the asymmetric ECS can surpass the SQL and reach the sub-Heisenberg limit.

III. QUANTUM PHASE SENSING UNDER DECOHERENCE

In this section, we study the quantum phase sensing in the presence of decoherence induced by photon loss. We shall calculate the QFI with decoherence and discuss the influence of the decoherence on the ultimate precision of the phase sensitivity. The photon loss can be modeled by inserting two identical beam splitters in each optical arm of the MZI phase

TABLE I. The QFI of the asymmetric ECS with respect to the total mean photon number $\bar{n}$ and its square $\bar{n}^2$ in the absence of photon loss ($R = 0$) when the asymmetric parameter is $k = 10$.

	$\bar{n}$								
	1.0	1.5	2	2.5	3	3.5	4.0	4.5	5.0
$\bar{n}^2$	1.00	2.25	4.00	6.25	9.00	12.25	16.00	20.25	25.00
F_Q	5.78	7.44	9.05	10.48	12.36	13.97	16.05	17.98	20.54

sensor with the following beam-splitter transformation:

$$\hat{B}_{r,r'}(\gamma) = \exp[i(\gamma/2)(\hat{a}_{r'}^{\dagger}\hat{a}_r + \hat{a}_r^{\dagger}\hat{a}_{r'})], \tag{16}$$

which couples two optical sensor modes $r = 1, 2$ to two environment modes $r' = 1, 2$ that are initially in the vacuum. The beam splitters transform the optical sensor mode into a linear combination of the optical sensor modes and environment modes:

$$\hat{B}_{r,r'}(\gamma)\hat{a}_r^{\dagger}\hat{B}_{r,r'}^{-1}(\gamma) = \sqrt{T}\hat{a}_r^{\dagger} + i\sqrt{R}\hat{a}_{r'}^{\dagger}, \tag{17}$$

where $T = \cos^2(\gamma/2)$ and $R = 1 - T$ are the transmission and loss rates of the photons, respectively. When $T = 1$ ($R = 0$), there is no photon loss in the interferometer, and when $T = 0$ ($R = 1$), all input photons leak out of the interferometer.

We consider the case in which the input sensor state is $|\Psi\rangle$ given by Eq. (1) while the two environment modes are in the vacuum state. We assume that the leaks in both arms have the same transmission coefficient T. Then the total output state of the sensor modes and environment modes before the second beam splitter is given by

$$|\Psi(\phi)\rangle = \hat{B}_{1,1'}(\gamma)\hat{B}_{2,2'}(\gamma)\hat{U}(\phi)|\Psi\rangle|0,0\rangle_{1',2'}, \tag{18}$$

where the phase-shift transformation is defined by $\hat{U}(\phi) = \exp[i\phi\hat{n}_2]$.

After the actions of the beam-splitter and phase-shift transformations, Eq. (18) becomes

$$\begin{aligned}|\Psi(\phi)\rangle = N[&|\sqrt{T}\alpha\rangle_1|i\sqrt{R}\alpha\rangle_{1'}\\ &\times|e^{i\phi}\sqrt{T}k\alpha\rangle_2|e^{i\phi}i\sqrt{R}k\alpha\rangle_{2'}\\ &+|-\sqrt{T}\alpha\rangle_1|-i\sqrt{R}\alpha\rangle_{1'}\\ &\times|-\sqrt{T}k\alpha e^{i\phi}\rangle_2|-i\sqrt{R}k\alpha e^{i\phi}\rangle_{2'}],\end{aligned} \tag{19}$$

which can be simply expressed as

$$\begin{aligned}|\Psi(\phi)\rangle = N_+[&|\phi_1(T)\rangle|i\sqrt{R}\alpha\rangle_{1'}|e^{i\phi}i\sqrt{R}k\alpha\rangle_{2'}\\ &+|\phi_2(T)\rangle|-i\sqrt{R}\alpha\rangle_{1'}|-i\sqrt{R}k\alpha e^{i\phi}\rangle_{2'}],\end{aligned} \tag{20}$$

where we have introduced two sensor-mode states.

$$\begin{aligned}|\phi_1(T)\rangle &= |\sqrt{T}\alpha\rangle_1|e^{i\phi}\sqrt{T}k\alpha\rangle_2,\\ |\phi_2(T)\rangle &= |-\sqrt{T}\alpha\rangle_1|-e^{i\phi}\sqrt{T}k\alpha\rangle_2,\end{aligned} \tag{21}$$

which satisfy the following nonorthogonal relation:

$$\langle\phi_1(T)|\phi_2(T)\rangle = e^{-2T(1+k^2)|\alpha|^2}. \tag{22}$$

In the presence of photon loss, the pure input state of the sensor modes will evolve to a mixed state. If the eigenvalues and eigenstates of the mixed state are known, the quantum Fisher information can be easily calculated by the use of the diagonalization method for a density matrix developed in Ref. [31]. The reduced density operator of the sensor modes is given by

$$\begin{aligned}\hat{\rho}(T) = N^2\big\{&|\phi_1(T)\rangle\langle\phi_1(T)| + |\phi_2(T)\rangle\langle\phi_2(T)|\\ &+2e^{-2R(1+k^2)|\alpha|^2}[|\phi_1(T)\rangle\langle\phi_2(T)| + \text{H.c.}]\big\}.\end{aligned} \tag{23}$$

Following the diagonalization method in Ref. [31], through some tedious calculations we can obtain the eigenvalues and eigenfunctions of the reduced density operator of the sensor modes:

$$\lambda_{\pm} = \tfrac{1}{2}(1 \pm \Lambda), \tag{24}$$

$$\Lambda = \sqrt{1 - N^4\big(1 - e^{-4T(1+k^2)|\alpha|^2}\big)\big(1 - e^{-4R(1+k^2)|\alpha|^2}\big)}. \tag{25}$$

Two orthogonal eigenfunctions of the reduced density operator are given by

$$\begin{aligned}|\lambda_{\pm}(\phi)\rangle = M_{\pm}(&\eta_{\pm}|\sqrt{T}\alpha\rangle_1|e^{i\phi}\sqrt{T}k\alpha\rangle_2\\ &+|-\sqrt{T}\alpha\rangle_1|-e^{i\phi}\sqrt{T}k\alpha\rangle_2),\end{aligned} \tag{26}$$

where the normalization constants are given by

$$M_{\pm} = \big[(1 + \eta_{\pm}^2) + 2\eta_{\pm}e^{-2T(1+k^2)|\alpha|^2}\big]^{-1/2}, \tag{27}$$

$$\eta_{\pm} = \frac{N^2\big[2e^{-2T(1+k^2)|\alpha|^2} + e^{-2R(1+k^2)|\alpha|^2}\big]}{2\lambda_{\pm} - N^2\big[2 + e^{-2(1+k^2)|\alpha|^2}\big]}. \tag{28}$$

Since the eigenvalues of the reduced density operator of the sensor modes are independent of the phase parameter ϕ, we can calculate the QFI by using the following formula [31]:

$$F_Q = \sum_{i=\pm}\lambda_i F_{Q,i} - \sum_{i\neq j}\frac{8\lambda_i\lambda_j}{\lambda_i + \lambda_j}\big|\langle\lambda_i'|\,\lambda_j\rangle\big|^2, \tag{29}$$

where the first term is the QFI of the eigenvalues of the reduced density operator of the sensor modes

$$F_{Q\pm} = 4(\langle\lambda_{\pm}'|\lambda_{\pm}'\rangle - |\langle\lambda_{\pm}'|\lambda_{\pm}\rangle|^2). \tag{30}$$

For convenience of calculation, we rewrite Eq. (29) as

$$\begin{aligned}F_Q = &[(F_{Q1,+} - F_{Q2,+}) + (F_{Q1,-} - F_{Q2,-})]\\ &-(F_{Q3,+} + F_{Q3,-}),\end{aligned} \tag{31}$$

where we introduce the following functions:

$$F_{Q1,\pm} = 4\lambda_{\pm}\langle\lambda_{\pm}'|\lambda_{\pm}'\rangle, \tag{32}$$

$$F_{Q2,\pm} = 4\lambda_{\pm}|\langle\lambda_{\pm}'|\lambda_{\pm}\rangle|^2, \tag{33}$$

$$F_{Q3,\pm} = \frac{8\lambda_+\lambda_-}{\lambda_+ + \lambda_-}|\langle\lambda_{\pm}'|\lambda_{\mp}\rangle|^2. \tag{34}$$

Making use of the eigenvalues and eigenfunctions of the reduced density operator given by Eqs. (24) and (26), we straightforwardly obtain

$$\begin{aligned}F_{Q1,\pm} = 4\lambda_{\pm}|M_{\pm}|^2Tk^2|\alpha|^2\big[&(1 + \eta_{\pm}^2)(1 + Tk^2|\alpha|^2)\\ &-2\eta_{\pm}(1 - Tk^2|\alpha|^2)e^{-2T(1+k^2)|\alpha|^2}\big],\end{aligned} \tag{35}$$

$$\begin{aligned}F_{Q2,\pm} = 4\lambda_{\pm}|M_{\pm}|^4T^2k^4|\alpha|^4\big[&(1 + \eta_{\pm}^2)\\ &-2\eta_{\pm}e^{-2T(1+k^2)|\alpha|^2}\big]^2,\end{aligned} \tag{36}$$

$$\begin{aligned}F_{Q3,\pm} = &\frac{8\lambda_+\lambda_-}{\lambda_+ + \lambda_-}|M_+|^2|M_-|^2T^2k^4|\alpha|^4\\ &\times|(1 + \eta_{\pm}\eta_{\mp}) - e^{-2T(1+k^2)|\alpha|^2}(\eta_{\pm} + \eta_{\mp})|^2.\end{aligned} \tag{37}$$

In what follows we numerically analyze the influence of the asymmetry in the asymmetric ECS on the phase-sensitive limit determined by the QFI given by Eq. (31). In Fig. 3, we plot the QFI with respect to the total mean photon number

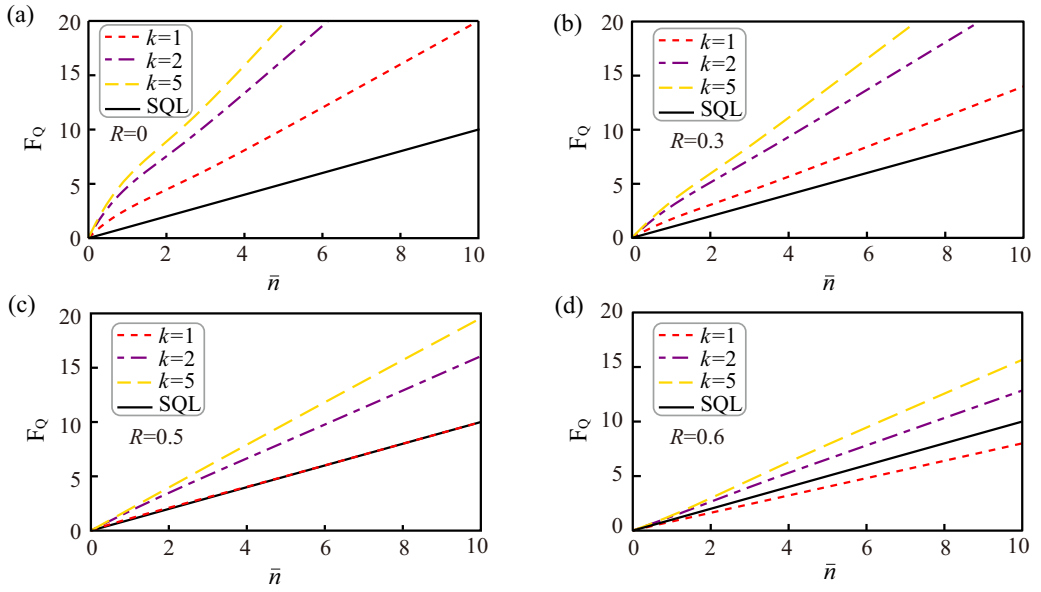

FIG. 3. The QFI with respect to the total mean photon number for different values of the asymmetric parameter k and the photon-loss rate R. (a) The asymmetric parameter takes $k = 1, 2, 3$, and the photon-loss rate $R = 0$. (b) The asymmetric parameter takes $k = 1, 2, 3$, and the photon-loss rate $R = 0.3$. (c) The asymmetric parameter takes $k = 1, 2, 3$, and the photon-loss rate $R = 0.5$. (d) The asymmetric parameter takes $k = 1, 2, 3$, and the photon-loss rate $R = 0.6$. The dotted, dot-dashed, and dashed lines correspond to the values of $k = 1, 2$, and 3, respectively.

for different values of the asymmetric parameter k in the presence of photon loss. The numerical simulation parameters are chosen to be the photon-loss rates $R = 0, 0.3, 0.5, 0.6$ for the symmetric ECS ($k = 1$) and the asymmetric ECS ($k = 2, 5$). The solid lines in Figs. 3(a)–3(d) denote the QFI corresponding to the SQL. The dashed lines show the QFI of the asymmetric-ECS case. The dotted lines denote the QFI of the symmetric-ECS case. Figures 3(a)–3(d) show that the QFI of the symmetric-ECS case decreases with the increase of photon loss. The QFI is larger than that of the SQL in the regime of smaller photon loss ($0 < R < 0.5$). The QFI is equal to that of the SQL when $R = 0.5$, while the QFI is smaller than that of the SQL in the regime of the larger photon loss ($R > 0.5$).

However, the situation is significantly different in the presence of the state asymmetry. The dash-dotted and dashed lines in Figs. 3(a)–3(d) represent the QFI when the asymmetric parameter is $k = 2$ and 5, respectively. In Figs. 3(a)–3(d) we can observe that the QFI of the asymmetric-ECS case is larger than that of the symmetric-ECS case and the SQL even in the presence of strong photon loss with $R = 0.6$.

We can, in detail, observe the ultraprecise limit of the asymmetric ECS in the phase estimation by comparing the QFI with values of $\bar{n}^2$. In Table II, we list some representative data for the QFI and the total mean photon number $\bar{n}$ and its square $\bar{n}^2$ when we take the photon-loss rate $R = 0.3$ and the asymmetric parameter $k = 2$. From the data in Table II, we can see that $F_Q > \bar{n}^2$, i.e., $\delta\phi_{\min} < 1/\bar{n}$, when $1 \leqslant \bar{n} \leqslant 2$. This implies that the phase-sensitivity limit of the asymmetric ECS can surpass the Heisenberg limit in the small-photon-number regime. Especially, it can be shown that the phase-sensitivity limit of the asymmetric ECS can also surpass the Heisenberg limit in the small-photon-number regime even in the case of strong photon loss. For instance, in the case of strong photon loss we find that $F_Q > \bar{n}^2$ and $\delta\phi_{\min} < 1/\bar{n}$ are still valid in the small-photon-number regime of $\bar{n} < 1.5$ when $R = 0.6$ and $k = 5$.

In order to further demonstrate the asymmetric advantage of the asymmetric ECS in the phase estimation, in Fig. 4 we numerically plot the QFI with respect to photon loss for the symmetric and asymmetric ECSs under the condition of the same input mean photon number $\bar{n} = 26$; therefore, the asymmetric parameter is $k = 1$, 2, 5, and the corresponding α is 3.60, 2.28, and 1.00, respectively. The dotted line is the symmetric-ECS case, while the dash-dotted and dashed lines corresponds to the asymmetric-ECS case with $k = 2$ and 5, respectively. From Fig. 4 we can see that the QFI of the asymmetric-ECS case is much larger than that of the symmetric-ECS case with the same photon loss. This implies that the asymmetric ECS has greater capability against photon loss. And the larger the asymmetric degree of the asymmetric ECS is, the greater the capability against photon loss is.

From the above numerical analyses we can conclude that the asymmetric ECS can exhibit a greater quantum advantage in the phase estimation over the symmetric ECS in the

TABLE II. The QFI of the asymmetric ECS with respect to the total mean photon number $\bar{n}$ and its square $\bar{n}^2$ in the presence of photon loss. We take the photon-loss rate $R = 0.3$ and the asymmetric parameter $k = 2$.

	$\bar{n}$								
	1.0	1.5	2.0	2.5	3.0	3.5	4.0	4.5	5.0
$\bar{n}^2$	1.00	2.25	4.00	6.25	9.00	12.25	16.00	20.25	25.00
F_Q	2.92	4.06	5.11	6.15	7.21	8.26	9.36	10.40	11.50

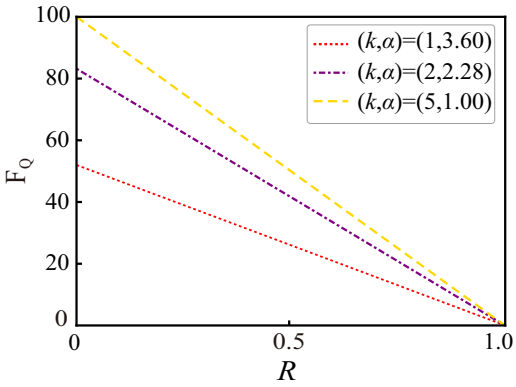

FIG. 4. The QFI with respect to the photon-loss rate R for different values of the asymmetric parameter k under the condition of the same input mean photon number $\bar{n} = 26$. The dotted line describes the case of the symmetric ECSs $(k, \alpha) = (1, 3.60)$. The dot-dashed and dashed lines denote the asymmetric-ECS cases $(k, \alpha) = (2, 2.28)$ and $(k, \alpha) = (5, 1.00)$, respectively.

presence of photon loss under the constraint of the same input mean photon number. First, the asymmetric ECS can create a better phase-sensitivity limit than the symmetric ECS. Second, the asymmetric ECS has a greater capability against the photon loss. In particular, in the regime of the small photon number the phase-sensitivity limit of the asymmetric ECS can also surpass the Heisenberg limit even in the environment with the strong photon loss.

IV. QUANTUM PHASE SENSING WITH INTENSITY-DIFFERENCE MEASUREMENT

In this section, we study the quantum phase sensing in a real measurement scheme. We consider the ultimate phase sensitivity with the MZI in the optical intensity-difference measurement given by the following intensity-difference operator:

$$\hat{S}_z = \tfrac{1}{2}(\hat{a}^\dagger \hat{a} - \hat{b}^\dagger \hat{b}). \tag{38}$$

The sensor output state after the second beam splitter is given by

$$\hat{\rho}_{\rm out}(\phi) = \hat{B}_{1,2}(\pi/2)\hat{\rho}(\phi)\hat{B}^\dagger_{1,2}(\pi/2), \tag{39}$$

where $\hat{B}_{1,2}(\pi/2)$ is the second 50:50 beam-splitter transformation in the MZI, and the reduced density matrix $\hat{\rho}(\phi)$ of the sensor modes is given by Eq. (23), which can be expressed as

$$\hat{\rho}(\phi) = \lambda_+ |\lambda_+(\phi)\rangle\langle\lambda_+(\phi)| + \lambda_- |\lambda_-(\phi)\rangle\langle\lambda_-(\phi)|. \tag{40}$$

It is straightforward to calculate the expectation value of the intensity-difference operator $\hat{S}_z$ in the output state $\hat{\rho}_{\rm out}$ of the MZI with the following result:

$$\begin{aligned}\langle\hat{S}_z\rangle &= \lambda_+\langle\lambda_+|\hat{B}^\dagger_{1,2}\hat{S}_z\hat{B}_{1,2}|\lambda_+\rangle + \lambda_-\langle\lambda_-|\hat{B}^\dagger_{1,2}\hat{S}_z\hat{B}_{1,2}|\lambda_-\rangle \\ &= S_{z,+} + S_{z,-},\end{aligned} \tag{41}$$

where $S_{z,\pm}$ is given by

$$S_{z,\pm} = -\lambda_\pm kT|\alpha|^2 \sin\phi M_+^2\left[(1+\eta_\pm^2) - 2\eta_\pm e^{-2T|\alpha|^2(k^2+1)}\right]. \tag{42}$$

Similarly, the expectation value of the operator $\hat{S}_z^2$ in the sensor output state $\hat{\rho}_{\rm out}$ can be obtained with the following expression:

$$\langle\hat{S}_z^2\rangle = S_{z2,+} + S_{z2,-}, \tag{43}$$

where $S_{z2,\pm}$ is given by

$$\begin{aligned}S_{z2,\pm} = {}& \lambda_\pm T^2|\alpha|^4k^2\sin^2\phi + \frac{\lambda_\pm}{4}|M_\pm|^2T|\alpha|^2(1+k^2) \\ &\times\left[(1+|\eta_\pm|^2) - e^{-2(1+k^2)|\alpha|^2}(\eta_\pm + \eta_\pm^*)\right].\end{aligned} \tag{44}$$

Hence, the phase sensitivity in the intensity-difference measurement scheme is given by the error transfer equation

$$\Delta\phi = \frac{\sqrt{\langle\hat{S}_z^2\rangle - \langle\hat{S}_z\rangle^2}}{|\partial\langle\hat{S}_z\rangle/\partial\phi|}. \tag{45}$$

In Fig. 5, under the condition of the same input mean photon number $\bar{n} = 26$ we plot the phase sensitivity in the intensity-difference-measurement scheme for different values of the asymmetric parameter $(k, \alpha) = (1, 3.60)$, $(k, \alpha) = (2, 2.28)$, and $(k, \alpha) = (5, 1.00)$. Figures 5(a) and 5(b) correspond to the two cases with and without photon loss, respectively. The solid lines in Fig. 5 denote the quantum Cramér-Rao bound given in the previous section. From Fig. 5 we can see that the phase sensitivity described by $\Delta\phi$ becomes better as the asymmetric parameter k increases for both the cases without and with photon loss, and it more closely approaches the quantum Cramér-Rao bound. Therefore, we can conclude that the asymmetry of the asymmetric ECS may enhance the phase sensitivity in the practical phase-measurement scheme.

Finally, we investigate the asymmetry-enhanced phase sensing by calculating the classical Fisher information for the above intensity-difference-measurement scheme. In general, the classical Fisher information determines the phase sensitivity once we have chosen a single specific measurement with positive operator-valued measure (POVM) elements. The POVM of the intensity-difference measurement is given by

$$\hat{\Pi}_{nm} = |n, m\rangle\langle n, m|, \tag{46}$$

where $|n, m\rangle$ is the eigenstate of the intensity-difference operator $\hat{S}_z$ defined in Eq. (38) with the eigenvalue $(n - m)/2$.

For simplicity, we consider the situation without photon loss. In this case, the sensor output state after the second beam splitter is given by

$$|\psi(\phi)\rangle_{\rm out} = \hat{B}_{12}(\pi/4)|\Psi(\phi)\rangle, \tag{47}$$

where $\hat{B}_{12}(\pi/4)$ is the 50:50 beam-splitter transformation and $|\Psi(\phi)\rangle$ is given by Eq. (3).

The conditional probability distribution associated with the specific measurement $\hat{S}_z$ is given by

$$P(S_z|\phi) = {\rm Tr}[\rho_{\rm out}(\phi)\hat{\Pi}_{nm}], \tag{48}$$

where the density operator of the sensor output state is given by $\rho_{\rm out}(\phi) = |\psi(\phi)\rangle_{\rm out}\langle\psi(\phi)|$.

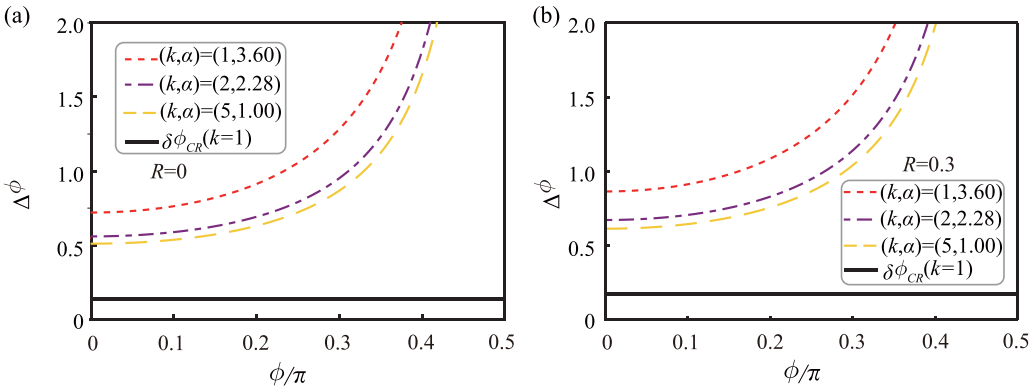

FIG. 5. The phase sensitivity in the intensity-difference measurement scheme for different values of the asymmetric parameter k and photon-loss rate R under the condition of the same input mean photon number $\bar{n} = 26$. (a) The case without photon loss. (b) The case in the presence of photon loss. Here the solid line denotes the corresponding quantum Cramér-Rao bound $\Delta\phi_{\rm CR}$ when $k = 1$ and $\bar{n} = 26$.

It is straightforward to get the conditional probability distribution and its derivative with the following expressions:

$$P_{n,m}(S_z|\phi) = 2N^2 e^{-(1+k^2)|\alpha|^2}[1+(-1)^{n+m}]\frac{I_+^n(\phi)I_-^m(\phi)}{n!m!}, \tag{49}$$

$$\frac{\partial P_{n,m}(S_z|\phi)}{\partial\phi} = 2k\cos\phi N^2|\alpha|^2 e^{-(1+k^2)|\alpha|^2}[1+(-1)^{n+m}] \times \frac{nI_+^{n-1}(\phi)I_-^m(\phi) - mI_+^n(\phi)I_-^{(m-1)}(\phi)}{n!m!}, \tag{50}$$

where N is the normalization constant given by Eq. (2) and we have introduced the following expressions:

$$I_\pm(\phi) = \tfrac{1}{2}|\alpha|^2(1 \pm 2k\sin\phi + k^2). \tag{51}$$

The classical Fisher information is given by the following expression:

$$F_c(\phi) = \sum_{n,m=0}^{\infty} \frac{1}{P_{n,m}(S_z|\phi)}\left(\frac{\partial P_{n,m}(S_z|\phi)}{\partial\phi}\right)^2, \tag{52}$$

from which we can obtain the classical Cramér-Rao bound of the phase sensitivity expressed in terms of the classical Fisher information [55]:

$$\Delta\phi_{\rm CCR} = \frac{1}{\sqrt{F_c}}. \tag{53}$$

Under the constraint of the same input mean photon number $\bar{n} = 26$, in Fig. 6 we plot the classical Cramér-Rao bound of the phase sensitivity in the intensity-difference measurement scheme when $\bar{n} = 26$ for the symmetric-ECS case $(k, \alpha) = (1, 3.60)$ and the asymmetric-ECS cases $(k, \alpha) = (2, 2.28)$ and $(k, \alpha) = (5, 1.00)$. From Fig. 6 we can see that the phase sensitivity of the asymmetric ECS is better than that of the symmetric ECS, and it becomes better as the asymmetric parameter k increases. Therefore, we can conclude that the asymmetry of the asymmetric ECS may enhance the phase sensitivity in the practical phase-measurement scheme. In Fig. 6, we also plot the corresponding quantum Cramér-Rao bound $\Delta\phi_{\rm CR}$ when $k = 1$ and $\bar{n} = 26$. From Fig. 6, it is straightforward that to see that the classical Cramér-Rao bound of the phase sensitivity in the intensity-difference measurement scheme is larger than the quantum Cramér-Rao bound under the condition of the same input mean photon number.

V. CONCLUSIONS

In this work, we have studied the quantum phase sensing with asymmetric two-mode ECSs via the MZI. We first investigated quantum phase sensing with the asymmetric ECS in the absence of photon loss. We showed that the asymmetry of the input asymmetric ECS can be used as a quantum resource to enhance the sensitivity of the quantum phase estimation. In particular, we found that the phase-sensitivity limit of the asymmetric ECS can reach and even surpass the Heisenberg limit in certain parameter regimes.

We then studied the quantum phase sensing with the asymmetric two-mode ECS under the effects of decoherence. We used an optical beam splitter to describe the photon loss. We showed that the asymmetric ECS can exhibit a quantum

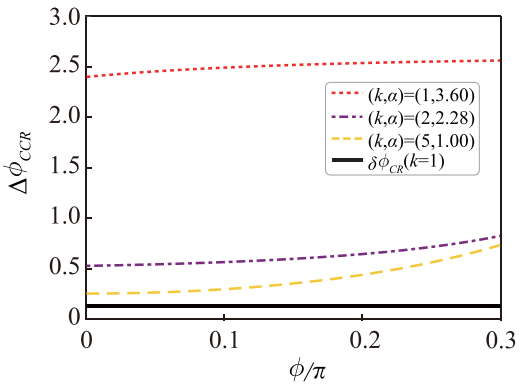

FIG. 6. The classical Cramér-Rao bound of the phase sensitivity in the intensity-difference measurement scheme for different values of the asymmetric parameter k under the condition of the same input mean photon number $\bar{n} = 26$. The dotted line describes the case of the symmetric ECSs $(k, \alpha) = (1, 3.60)$. The dot-dashed and dashed lines denote the asymmetric-ECS cases $(k, \alpha) = (2, 2.28)$ and $(k, \alpha) = (5, 1.00)$, respectively. Here the solid line denotes the corresponding quantum Cramér-Rao bound $\Delta\phi_{\rm CR}$ when $k = 1$ and $\bar{n} = 26$.

advantage in phase sensing over the symmetric ECS in the presence of photon loss. We found that the asymmetric ECS not only can create a better phase sensitivity limit than the symmetric ECS but can also have greater capability against photon loss. In particular, in the regime of the small photon number the phase-sensitivity limit of the asymmetric ECS can also surpass the Heisenberg limit even in the environment with strong photon loss.

We also investigated quantum phase sensing in a practical measurement scheme with asymmetric two-mode ECSs. As a concrete example, we studied phase sensitivity with the MZI in the optical intensity-difference-measurement scheme. We found that the asymmetry in the asymmetric ECS can significantly enhance the phase sensitivity in the practical phase-measurement scheme. In summary, our results reveal that the asymmetry in the asymmetric ECS is a quantum-sensing resource, and the present work may be applied to ultrasensitive quantum phase sensing in the presence of photon loss.

ACKNOWLEDGMENTS

L.-M.K. is supported by the Natural Science Foundation of China (NSFC; Grants No. 12247105, No. 12175060, and No. 11935006), the Hunan provincial sci-tech program (Grants No. 2020RC4047 and No. 2023ZJ1010), and the XJ-Lab key project (Grant No. 23XJ02001). W.-J.L. is supported by the NSFC (Grant No. 12205092). Y.-F.J. is supported by the NSFC (Grant No. 12147156), the China Postdoctoral Science Foundation (Grants No. 2021M701176 and No. 2022T150208), and the Science and Technology Innovation Program of Hunan Province (Grant No. 2021RC2078).

X.T.C. and R.Z. contributed equally to this work.

[1] B. Yurke and D. Stoler, Generating quantum mechanical superpositions of macroscopically distinguishable states via amplitude dispersion, Phys. Rev. Lett. **57**, 13 (1986).

[2] A. Mecozzi and P. Tombesi, Distinguishable quantum states generated via nonlinear birefringence, Phys. Rev. Lett. **58**, 1055 (1987).

[3] B. C. Sanders, Entangled coherent states, Phys. Rev. A **45**, 6811 (1992); Erratum: Entangled coherent states [Phys. Rev. A **45**, 6811 (1992)], **46**, 2966(E) (1992).

[4] B. C. Sanders, Review of entangled coherent states, J. Phys. A **45**, 244002 (2012).

[5] B. C. Sanders, S. D. Bartlett, T. Rudolph, and P. L. Knight, Photon-number superselection and the entangled coherent-state representation, Phys. Rev. A **68**, 042329 (2003).

[6] H. Jeong, M. Paternostro, and T. C. Ralph, Failure of local realism revealed by extremely-coarse-grained measurements, Phys. Rev. Lett. **102**, 060403 (2009).

[7] B. T. Kirby and J. D. Franson, Macroscopic state interferometry over large distances using state discrimination, Phys. Rev. A **89**, 033861 (2014).

[8] C.-Y. Park and H. Jeong, Bell-inequality tests using asymmetric entangled coherent states in asymmetric lossy environments, Phys. Rev. A **91**, 042328 (2015).

[9] M. Paternostro and H. Jeong, Testing nonlocal realism with entangled coherent states, Phys. Rev. A **81**, 032115 (2010).

[10] C. W. Lee, M. Paternostro, and H. Jeong, Faithful test of nonlocal realism with entangled coherent states, Phys. Rev. A **83**, 022102 (2011).

[11] X. Wang, Quantum teleportation of entangled coherent states, Phys. Rev. A **64**, 022302 (2001).

[12] S. J. van Enk and O. Hirota, Entangled coherent states: Teleportation and decoherence, Phys. Rev. A **64**, 022313 (2001).

[13] H. Jeong, M. S. Kim, and J. Lee, Quantum-information processing for a coherent superposition state via a mixed entangled coherent channel, Phys. Rev. A **64**, 052308 (2001).

[14] H. Jeong and M. S. Kim, Purification of entangled coherent states, Quantum Inf. Comput. **2**, 208 (2002).

[15] N. B. An, Teleportation of coherent-state superpositions within a network, Phys. Rev. A **68**, 022321 (2003).

[16] P. T. Cochrane, G. J. Milburn, and W. J. Munro, Macroscopically distinct quantum-superposition states as a bosonic code for amplitude damping, Phys. Rev. A **59**, 2631 (1999).

[17] H. Jeong and M. S. Kim, Efficient quantum computation using coherent states, Phys. Rev. A **65**, 042305 (2002).

[18] T. C. Ralph, A. Gilchrist, G. J. Milburn, W. J. Munro, and S. Glancy, Quantum computation with optical coherent states, Phys. Rev. A **68**, 042319 (2003).

[19] A. P. Lund, T. C. Ralph, and H. L. Haselgrove, Fault-tolerant linear optical quantum computing with small-amplitude coherent states, Phys. Rev. Lett. **100**, 030503 (2008).

[20] P. Marek and J. Fiurášek, Elementary gates for quantum information with superposed coherent states, Phys. Rev. A **82**, 014304 (2010).

[21] C. R. Myers and T. C. Ralph, Coherent state topological cluster state production, New J. Phys. **13**, 115015 (2011).

[22] J. Kim, J. Lee, S.-W. Ji, H. Nha, P. M. Anisimov, and J. P. Dowling, Coherent-state optical qudit cluster state generation and teleportation via homodyne detection, Opt. Commun. **337**, 79 (2015).

[23] D. S. Simon, G. Jaeger, and A. V. Sergienko, Entangled coherent-state quantum key distribution with entanglement witnessing, Phys. Rev. A **89**, 012315 (2014).

[24] C. C. Gerry and R. A. Campos, Generation of maximally entangled photonic states with a quantum-optical Fredkin gate, Phys. Rev. A **64**, 063814 (2001).

[25] C. C. Gerry, A. Benmoussa, and R. A. Campos, Nonlinear interferometer as a resource for maximally entangled photonic states: Application to interferometry, Phys. Rev. A **66**, 013804 (2002).

[26] W. J. Munro, K. Nemoto, G. J. Milburn, and S. L. Braunstein, Weak-force detection with superposed coherent states, Phys. Rev. A **66**, 023819 (2002).

[27] R. A. Campos, C. C. Gerry, and A. Benmoussa, Optical interferometry at the Heisenberg limit with twin Fock states and parity measurements, Phys. Rev. A **68**, 023810 (2003).

[28] J. Joo, W. J. Munro, and T. P. Spiller, Quantum metrology with entangled coherent states, Phys. Rev. Lett. **107**, 083601 (2011).

[29] O. Hirota, K. Kato, and D. Murakami, Effectiveness of entangled coherent state in quantum metrology, arXiv:1108.1517.
[30] J. Joo, K. Park, H. Jeong, W. J. Munro, K. Nemoto, and T. P. Spiller, Quantum metrology for nonlinear phase shifts with entangled coherent states, Phys. Rev. A **86**, 043828 (2012).
[31] Y. M. Zhang, X. W. Li, W. Yang, and G. R. Jin, Quantum Fisher information of entangled coherent states in the presence of photon loss, Phys. Rev. A **88**, 043832 (2013).
[32] S.-Y. Lee, Y. S. Ihn, and Z. Kim, Optimal entangled coherent states in lossy quantum-enhanced metrology, Phys. Rev. A **101**, 012332 (2020).
[33] A. Ourjoumtsev, F. Ferreyrol, R. Tualle-Brouri, and P. Grangier, Preparation of non-local superpositions of quasi-classical light states, Nat. Phys. **5**, 189 (2009).
[34] J. C. Howell and J. A. Yeazell, Entangling macroscopic quantum states, Phys. Rev. A **62**, 012102 (2000).
[35] B. Yurke and D. Stoler, Quantum behavior of a four-wave mixer operated in a nonlinear regime, Phys. Rev. A **35**, 4846 (1987).
[36] P. Tombesi and A. Mecozzi, Generation of macroscopically distinguishable quantum states and detection by the squeezed-vacuum technique, J. Opt. Soc. Am. B **4**, 1700 (1987).
[37] C. C. Gerry, Generation of Schrödinger cats and entangled coherent states in the motion of a trapped ion by a dispersive interaction, Phys. Rev. A **55**, 2478 (1997).
[38] B. C. Sanders and D. A. Rice, A description of the quantised nonlinear interferometer, Opt. Quant. Electron. **31**, 525 (1999).
[39] B. C. Sanders and D. A. Rice, Nonclassical fields and the nonlinear interferometer, Phys. Rev. A **61**, 013805 (1999).
[40] Z. M. Liu and L. Zhou, An asymmetrical entangled coherent state: Generation scheme and nonclassical properties, Optik **142**, 1 (2017).
[41] S. J. van Enk, Entanglement capabilities in infinite dimensions: Multidimensional entangled coherent states, Phys. Rev. Lett. **91**, 017902 (2003).
[42] L. M. Kuang and L. Zhou, Generation of atom-photon entangled states in atomic Bose-Einstein condensate via electromagnetically induced transparency, Phys. Rev. A **68**, 043606 (2003).
[43] L. M. Kuang, Z. B. Chen, and J. W. Pan, Generation of entangled coherent states for distant Bose-Einstein condensates via electromagnetically induced transparency, Phys. Rev. A **76**, 052324 (2007).
[44] M. Sisodia, C. Shukla, and G. L. Long, Linear optics-based entanglement concentration protocols for cluster-type entangled coherent state, Quantum Inf. Process. **18**, 253 (2019)
[45] B. Li, W. Qin, Y. F. Jiao, C. L. Zhai, X. W. Xu, L. M. Kuang, and H. Jing, Optomechanical Schrödinger cat states in a cavity Bose-Einstein condensate, Fundam. Res. **3**, 15 (2023).
[46] Y. F. Jiao, J. X. Liu, Y. Li, R. Yang, L. M. Kuang, and H. Jing, Nonreciprocal enhancement of remote entanglement between nonidentical mechanical oscillators, Phys. Rev. Appl. **18**, 064008 (2022).
[47] Y.-F. Jiao, S.-D. Zhang, Y.-L. Zhang, A. Miranowicz, L. M. Kuang, and H. Jing, Nonreciprocal optomechanical entanglement against backscattering loss, Phys. Rev. Lett. **125**, 143605 (2020).
[48] J.-Q. Liao, Q.-Q. Wu, and F. Nori, Entangling two macroscopic mechanical mirrors in a two-cavity optomechanical system, Phys. Rev. A **89**, 014302 (2014).
[49] V. Giovannetti, S. Lloyd, and L. Maccone, Advances in quantum metrology, Nat. Photon. **5**, 222 (2011).
[50] V. Giovannetti, S. Lloyd, and L. Maccone, Quantum enhanced measurements: Beating the standard quantum limit, Science **306**, 1330 (2004).
[51] V. Giovannetti, S. Lloyd, and L. Maccone, Quantum metrology, Phys. Rev. Lett. **96**, 010401 (2006).
[52] G. Tóth and I. Apellaniz, Quantum metrology from a quantum information science perspective, J. Phys. A **47**, 424006 (2014).
[53] C. L. Degen, F. Reinhard, and P. Cappellaro, Quantum sensing, Rev. Mod. Phys. **89**, 035002 (2017).
[54] S. Pirandola, B. R. Bardhan, T. Gehring, C. Weedbrook, and S. Lloyd, Advances in photonic quantum sensing, Nat. Photon. **12**, 724 (2018).
[55] M. Barbieri, Optical quantum metrology, PRX Quantum **3**, 010202 (2022).
[56] H. Kwon, K. C. Tan, T. Volkoff, and H. Jeong, Nonclassicality as a quantifiable resource for quantum metrology, Phys. Rev. Lett. **122**, 040503 (2019).
[57] K. Gietka and H. Ritsch, Squeezing and overcoming the Heisenberg scaling with spin-orbit coupled quantum gases, Phys. Rev. Lett. **130**, 090802 (2023).
[58] J. A. H. Nielsen, J. S. Neergaard-Nielsen, T. Gehring, and U. L. Andersen, Deterministic quantum phase estimation beyond N00N states, Phys. Rev. Lett. **130**, 123603 (2023).
[59] S. Hao, H. Shi, C. N. Gagatsos, M. Mishra, B. Bash, I. Djordjevic, S. Guha, Q. Zhuang, and Z. Zhang, Demonstration of entanglement-enhanced covert sensing, Phys. Rev. Lett. **129**, 010501 (2022).
[60] N. Lupu-Gladstein, Y. Batuhan Yilmaz, D. R. M. Arvidsson-Shukur, A. Brodutch, A. O. T. Pang, A. M. Steinberg, and N. Y. Halpern, Negative quasiprobabilities enhance phase estimation in quantum-optics experiment, Phys. Rev. Lett. **128**, 220504 (2022)
[61] L. Maccone and C. Ren, Quantum radar, Phys. Rev. Lett. **124**, 200503 (2020).
[62] Q. Zhuang, Quantum ranging with gaussian entanglement, Phys. Rev. Lett. **126**, 240501 (2021).
[63] X. Zuo, Z. Yan, Y. Feng, J. Ma, X. Jia, C. Xie, and K. Peng, Quantum interferometer combining squeezing and parametric amplification, Phys. Rev. Lett. **124**, 173602 (2020).
[64] W. Wu and J.-H. An, Gaussian quantum metrology in a dissipative environment, Phys. Rev. A **104**, 042609 (2021).
[65] C. Chen, P. Wang, and R.-B. Liu, Effects of local decoherence on quantum critical metrology, Phys. Rev. A **104**, L020601 (2021).
[66] Y. Chu, S. Zhang, B. Yu, and J. Cai, Dynamic framework for criticality-enhanced quantum sensing, Phys. Rev. Lett. **126**, 010502 (2021).
[67] Y. Chu, Y. Liu, H. Liu, and J. Cai, Quantum sensing with a single-qubit pseudo-Hermitian system, Phys. Rev. Lett. **124**, 020501 (2020).
[68] F. Belliardo and V. Giovannetti, Achieving Heisenberg scaling with maximally entangled states: An analytic upper bound for the attainable root-mean-square error, Phys. Rev. A **102**, 042613 (2020).
[69] Q. S. Tan, J. B. Yuan, G. R. Jin, and L. M. Kuang, Near-Heisenberg-limited parameter estimation precision by

a dipolar-Bose-gas reservoir engineering, Phys. Rev. A **96**, 063614 (2017).

[70] H. Lü, S. K. Özdemir, L. M. Kuang, F. Nori, and H. Jing, Exceptional points in random-defect phonon lasers, Phys. Rev. Appl. **8**, 044020 (2017).

[71] Q. S. Tan, W. Wu, L. Xu, J. Liu, and L. M. Kuang, Quantum sensing of supersensitivity for the Ohmic quantum reservoir, Phys. Rev. A **106**, 032602 (2022).

[72] W. J. Lu, Z. Li, and L. M. Kuang, Nonlinear Dicke quantum Phase transition and its quantum witness in a cavity-Bose-Einstein-condensate system, Chin. Phys. Lett. **35**, 116401 (2018).

[73] Y. Gao and L. M. Kuang, Optimal quantum estimation of the displacement in optical imaging, J. Phys. B **52**, 215403 (2019).

[74] Y. Gao and L. M. Kuang, Quantum limits on the force sensitivity of a linear detector with linear measurements, Opt. Commun. **463**, 125377 (2020).

[75] Q. S. Tan, J. B. Yuan, J. Q. Liao, and L. M. Kuang, Supersensitive estimation of the coupling rate in cavity optomechanics with an impurity-doped Bose-Einstein condensate, Opt. Express **28**, 22867 (2020).

[76] W. Zhao, S. D. Zhang, A. Miranowicz, and H. Jing, Weak-force sensing with squeezed optomechanics, Sci. China: Phys., Mech. Astron. **63**, 224211 (2020).

[77] H. Jing, H. Lü, Ş. K. Özdemir, T. Carmon, and F. Nori, Nanoparticle sensing with a spinning resonator, Optica **5**, 1424 (2018).

[78] C. M. Caves, Quantum-mechanical noise in an interferometer, Phys. Rev. D **23**, 1693 (1981).

[79] The LIGO Scientific Collaboration, A gravitational wave observatory operating beyond the quantum shot-noise limit, Nat. Phys. **7**, 962 (2011).

[80] J. Aasi *et al.*, Enhanced sensitivity of the LIGO gravitational wave detector by using squeezed states of light, Nat. Photon. **7**, 613 (2013).

[81] J. P. Dowling, Quantum optical metrology – the lowdown on high-N00N states, Contemp. Phys. **49**, 125 (2008).

[82] A. N. Boto, P. Kok, D. S. Abrams, S. L. Braunstein, C. P. Williams, and J. P. Dowling, Quantum interferometric optical lithography: Exploiting entanglement to beat the diffraction limit, Phys. Rev. Lett. **85**, 2733 (2000).

[83] P. Kok, A. N. Boto, D. S. Abrams, C. P. Williams, S. L. Braunstein, and J. P. Dowling, Quantum-interferometric optical lithography: Towards arbitrary two-dimensional patterns, Phys. Rev. A **63**, 063407 (2001).

[84] P. M. Anisimov, G. M. Raterman, A. Chiruvelli, W. N. Plick, S. D. Huver, H. Lee, and J. P. Dowling, Quantum metrology with two-mode squeezed vacuum: Parity detection beats the Heisenberg limit, Phys. Rev. Lett. **104**, 103602 (2010).

[85] L. Pezzé and A. Smerzi, Ultrasensitive two-mode interferometry with single-mode number squeezing, Phys. Rev. Lett. **110**, 163604 (2013).